Available online at www.sciencedirect.com

SciVerse ScienceDirect

Ceramics International 39 (2013) 2527–2533

CERAMICS INTERNATIONAL

www.elsevier.com/locate/ceramint

Effects of powder size and metallic bonding layer on corrosion behaviour of plasma-sprayed Al_2O_3-13% TiO_2 coated mild steel in fresh tropical seawater

N.H.N. Yusoff[a], M.J. Ghazali[b,*], M.C. Isa[a], A.R. Daud[c], A. Muchtar[b]

[a] *Maritime Technology Division, Science And Technology Research Institute For Defence (STRIDE), c/o KD MALAYA, 32100 Pangkalan TLDM, Lumut, Perak, Malaysia*

[b] *Department. of Mechanical & Materials Engineering, Faculty of Engineering & Built Environment, University Kebangsaan Malaysia, 43600 UKM, Bangi, Selangor, Malaysia*

[c] *School of Applied Physics, Faculty of Science & Technology, Universiti Kebangsaan Malaysia, 43600 UKM, Bangi, Selangor, Malaysia*

Received 24 July 2012; received in revised form 3 September 2012; accepted 4 September 2012
Available online 12 September 2012

Abstract

This study focuses on the effects of powder size and Ni–Al bonding layer on the electrochemical behaviour of plasma-sprayed Al_2O_3-13% TiO_2 coating in fresh tropical seawater. The presence of the metallic bonding layer reduces the coating porosity and increases the surface roughness for both microparticle and nanoparticle coatings. The nanoparticle exhibits better corrosion rate of 1.9×10^{-6} mmpy compared to the microparticle coating, with a corrosion rate of 3.05×10^{-6} mmpy. However, the presence of the metallic bonding layer increases the corrosion rate for both micro and nanoparticle coatings. The corrosion mechanism for the coating with and without the metallic bonding layer is discussed in detail.

Keywords: C. Corrosion; D. Al_2O_3; D. TiO_2; E. Structural applications

1. Introduction

Many facilities located close to a marine environment suffer from corrosion attacks throughout their services [1,2]. Methods such as cathodic protection technique, corrosion inhibitor, and surface coating are used to reduce the corrosion rates and protect any type of metal-based structure from severe corrosion attacks. One of the common techniques used to prevent corrosion is by depositing a protective coating onto the metal surface. Ceramics coating for example, has shown its ability to be used where corrosion and wear co-exist, especially at an elevated temperature [3]. Recently, alumina titania (Al_2O_3–TiO_2) coatings have been reported to be very important because of their excellent wear, corrosion, and erosion resistance [4–6]. Early research on these coatings only focused on their microstructures and phase transformations. However, the interest of researchers has now shifted to mechanical properties and their relation to microstructures [7]. Plasma-sprayed Al_2O_3–TiO_2 is widely used as wear resistance coating in textile, machinery, and printing industries [8]. This process involves melting a feedstock material and rapidly transporting the resulting molten particles so as to "splat" against a substrate surface. Upon impact onto the substrate, the particles spread out and solidify to build up a layered arrangement of splats. The resulting laminar microstructure is highly defective with weak interfaces and voids between splats, as well as unmelted particles and cracks [9]. When plasma-sprayed Al_2O_3–TiO_2 coating is applied in aggressive media, electrolyte can penetrate the coating through permeable defects such as pores, cracks, and grain boundaries. The interaction between the electrolyte and metal surface can provide the corrosion reaction [10,11]. Thus, Al_2O_3–TiO_2 internal microstructures play a big role in providing corrosion protection as to prevent or reduce corrosion attacks.

*Corresponding author. Tel./fax: +60 38 925 9659.
E-mail address: mariyam@eng.ukm.my (M.J. Ghazali).

0272-8842/$ - see front matter © 2012 Elsevier Ltd and Techna Group S.r.l. All rights reserved.
http://dx.doi.org/10.1016/j.ceramint.2012.09.012

It is well known that one of the main concerns when applying the ceramic coating is the adhesion between the substrate and the coating. In order to improve the adhesion strength, a metallic coating that acts as a metallic bonding layer was proposed in this study [12]. The main mechanism of the coating–substrate adhesion in conventional plasma spraying is via mechanical interlocking in which the irregularities on rough surfaces are filled with the spreading molten materials due to the impact pressure. The subsequent solidification leads to mechanical interlocking. Mismatch between the thermal expansion coefficients of ceramic and metals leads to the development of excessive stresses at the interface, which is the main problem in metal–ceramic joining [13–15]. This is a common problem for depositing ceramic coating on metals. Thus, a metallic bonding layer application is normally utilised in order to give a better effect to the mechanical properties. However, further study for application in the aggressive media such as marine environment is still needed.

The current work aims to study the effects of the powder size and metallic bonding layer on the electrochemical behaviour of plasma-sprayed Al_2O_3-13% TiO_2 coating in fresh tropical seawater. Based on these results, an attempt will be made to correlate the corrosion parameters of Al_2O_3-13% TiO_2 coating with and without the metallic bonding layer.

2. Materials and methods

Prior to the deposition process, a mild steel substrate was degreased and grit-blasted with alumina to obtain a rough surface (~4.5 μm) and sufficient contact points between the coated material and the substrate. The Ni–Al coating layer, with a thickness of around 30 μm, is applied to the treated substrate surface act as a bonding layer by plasma spraying.

Two types of Al_2O_3-13% TiO_2 powder feedstock were used in the study; microparticle Al_2O_3-13% TiO_2 powders with a grain size of 10–25 μm (HAI Advanced Material Specialists, Inc.) and agglomerated nanoparticle powders with a grain size of 20–60 μm (Inframat Advanced Materials). The microparticle feedstock was manufactured through the so-called cladding process in which fused and crushed Al_2O_3 powders were clad with TiO_2 [6]. Morphology of the two types of powder feedstock is shown in Fig. 1.

The microparticle feedstock shows an irregular shape, whereas the agglomerated nanoparticle feedstock shows a round shape that consists of submicron particles. The series of coatings was applied to the substrate using the SG-100 Plasma Spray Gun (Praxair) mounted on a programmable robot. All samples with and without metallic bonding layers were labelled accordingly as shown in Table 1. The morphology of as-sprayed coating surface was observed under a LEO 1430 VP scanning electron microscope (SEM). The roughness of the coating surface was measured using a Formtracer SV-C3100 (Mitutoyo).

For the electrochemical study, the samples were soldered onto the outer surface without any coating, with a copper conducting wire. Then, the samples were clad with cold mounting, leaving only an exposed area of coating of about 1.8 cm^2. Before the corrosion test, the samples were washed with distilled water, degreased with acetone, and dried. The electrochemical corrosion test of the coating samples was performed in a three-electrode cell using a graphite electrode as a counter electrode, a saturated calomel electrode (SCE) as a reference electrode, and the coated sample as the working electrode. Fresh tropical seawater was used as a test solution, which was maintained at room temperature.

Electrochemical tests were conducted using a PC4/750 Galvanostat/Potentiostat (Gamry Instruments, Inc). A potentiodynamic polarisation investigation of coated samples was performed with a scan rate of 0.5 mV/s and a potential range of $\pm$250 mV vs. SCE with reference to corrosion potential. The collected information was analysed using the Echem Analyst V1.2 software. Electrochemical impedance spectroscopy (EIS) of the coated samples was measured using a signal amplitude of 5 mV with a measurement frequency range of 0.01–100,000 Hz. The measured EIS

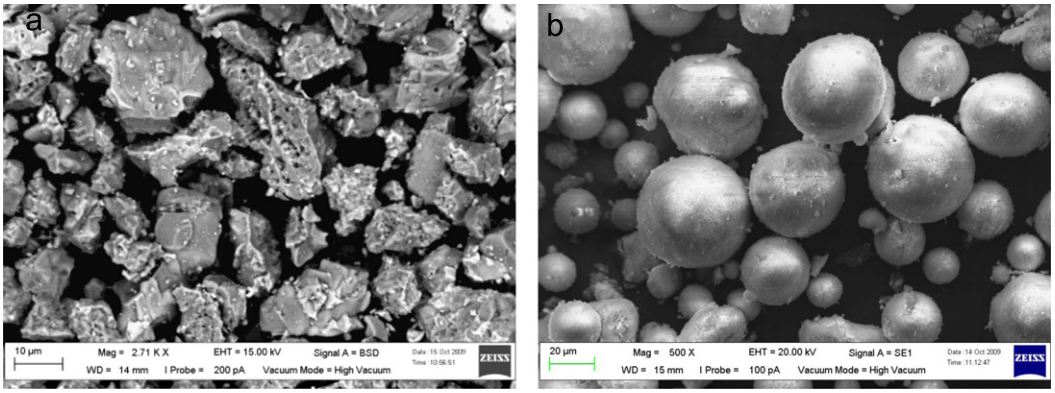

Fig. 1. SEM image of the feedstock morphology for (a) microparticle and (b) agglomerated nanoparticle Al_2O_3-13% TiO_2 powder.

Table 1
Spray parameters for Ni–Al metallic bonding layer and Al_2O_3-13% TiO_2 coating.

Spray parameters	Unit	Bonding layer	Al_2O_3-13% TiO_2 layer			
			M1	M2	N1	N2
Plasma power	kW	30	35	35	30	30
Primary gas pressure	Psi	50	100	100	40	40
Secondary gas pressure	Psi	60	60	60	60	60
Carrier gas pressure	Psi	30	40	40	20	20
Powder feed rate	*Rpm*	1	1	1	3	3
Coating speed	mm/s	250	250	250	250	250
Layer	Cycle	2	10	10	10	10
Pre-heat	Cycle	2	2	2	2	2
Spray distance	mm	100	100	100	100	100

M1-microparticles without the bonding layer.
M2-microparticles with the bonding layer.
N1-microparticles without the bonding layer.
N2-microparticles with the bonding layer.

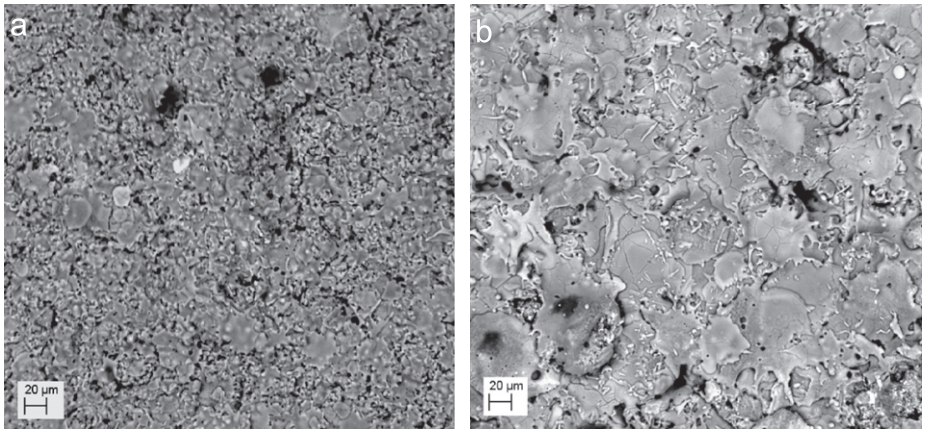

Fig. 2. SEM image of Al_2O_3-13% TiO_2 coating surface for (a) microparticle and (b) nanoparticle coating.

data were fitted and interpreted using the Gamry EIS 300 software.

3. Results and discussion

3.1. Microstructure

Fig. 2(a and b) show the surface morphologies of micro and nanoparticle Al_2O_3-13% TiO_2 coatings, respectively with metallic bonding layers. Evidently, the Al_2O_3-13% TiO_2 coatings exhibit lamellar splat structures. The structure was formed during plasma spraying when the molten droplets strike the substrate at a high velocity, resulting in splat morphology [16]. The splat size of microparticle coatings is slightly smaller than that of nanoparticle coatings because of a denser feedstock powder. By providing a small droplet splat, the microparticle coatings show an increment in voids or pores from the splat boundaries appearing as a black area, as shown in Fig. 2(a).

Fig. 3(a and b) show the SEM images of the coating cross-section for the microparticle and nanoparticle coatings with metallic bonding layers. The microparticle feedstock exhibits coating with more pores randomly distributed in the partially melted region, which is most likely caused by an imperfect contact with partially melted ceramic particles or gas entrapment formation [17]. In contrast, the nanoparticle feedstock provides coatings with low pores through the alternately built partially melted region and fully melted region. In some areas, the two regions are combined without distinct boundaries. This microstructure is anticipated and can provide a better coating performance consistent with the observation in previous studies on nanostructure coating produced using nanocrystalline feedstock [8,18–20]. The low percentages of pores contributed by both micro and nanoparticle feedstock are confirmed based on image analysis measurement, as shown in Table 2. The presence of the metallic bonding layer also reduced the coating porosity between the microparticle (i.e., M1 and M2) and nanoparticle coatings (i.e., N1 and N2) for a better thermal expansion between the metallic bonding layer and the Al_2O_3-13% TiO_2 coating. These pores and microcracks were formed because of the

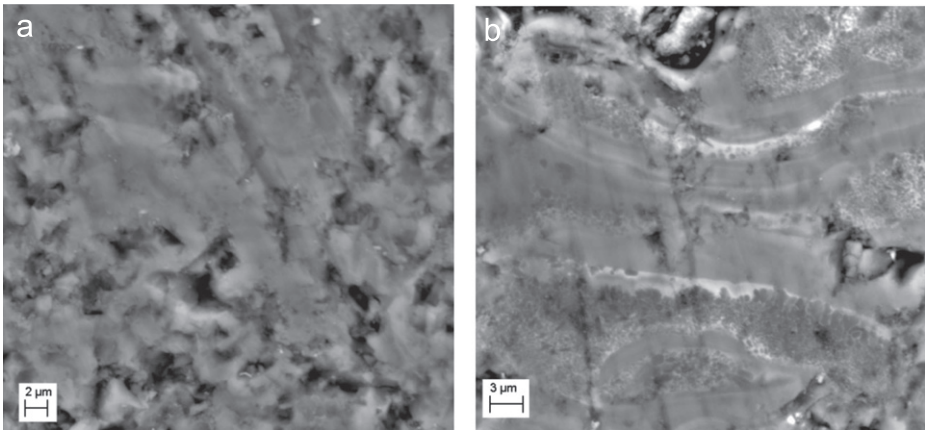

Fig. 3. SEM image of the Al_2O_3-13% TiO_2 coating cross-section for (a) microparticle and (b) nanoparticle coating.

Table 2
The surface roughness and the percentage of coating porosity with and without Ni–Al bonding layer.

	R_a (µm)	% Pores
M1	3.70	8.6
M2	4.30	6.3
N1	6.83	5.0
N2	7.70	3.9

tensile residual stress (quenching stress) generated during the rapid cooling process of the droplets when they spread out over the substrate [9]. The presence of the metallic bonding layer increased the surface roughness of the coating using either the microparticle or the nanoparticle feedstock. This behaviour is caused by the particle size of the metallic bonding layer that is relatively large and produces a the coarser surface [21].

3.2. Corrosion behaviour

The electrochemical behaviour of the mild steel substrate was evaluated by the Tafel extrapolation technique to measure the corrosion rate in a tropical marine environment. The corrosion potential (E_{cor}) and corrosion current density (i_{cor}) values were extracted from the Tafel plot, as shown in Fig. 4. The corrosion rate was determined using a software based on Eq. (1) [22]. The collected and analysed data are presented in Table 3.

$$\text{Corrosion rate (mm/year)} = \frac{3.27EWi_{cor}}{dA} \quad (1)$$

where EW=equivalent weight (g/equivalent), d=density (g/cm^3), A=sample area (cm^2).

The microparticle without metallic bonding layer yielded a corrosion rate of 3.05×10^{-6} mmpy, whereas the nanoparticle without metallic bonding layer yielded 1.9×10^{-6} mmpy. The nanoparticle without metallic bonding layer with smaller particle size is shown to provide better protection to mild steel when exposed to the marine environment. The higher

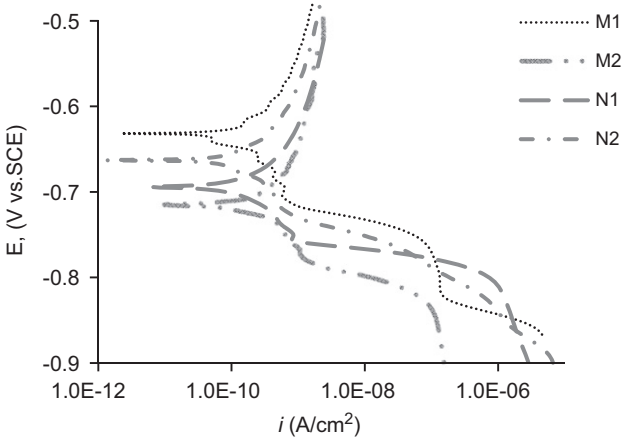

Fig. 4. Tafel plot for coated sample M1, M2, N1 and N2.

corrosion rate of the microparticle without metallic bonding layer sample compared with that of the nanoparticle without metallic bonding layer sample was caused by the high coating EW, which resulted from the denser feedstock powder of the microparticle coating. The results agreed with those of the previous study by Tian et al. and Yang et al., which found nanoparticle coatings to provide better corrosion protection than microparticle coatings [1,11].

The present study also found that the presence of a metallic bonding layer caused an increment in the corrosion rate. As shown in Table 3, the microparticle with metallic bonding layer gives a higher corrosion rate than the microparticle without metallic bonding layer, whereas the nanoparticle with metallic bonding layer provides a higher corrosion rate than the nanoparticle without metallic bonding layer. This occurrence was caused by the high I_{cor} contributed by the metallic bonding layer, which decreased the corrosion resistance of the coating [1].

3.3. Electrochemistry impedance studies

The EIS characteristics of Al_2O_3-13% TiO_2 in fresh seawater were examined at the open circuit potential after

Table 3
The corrosion parameters of the coating extract from the Tafel plot.

	Samples			
	M1	**M2**	**N1**	**N2**
I_{cor} (nA/cm^2)	0.5	5.2	1.2	1.7
E_{cor} (mV)	−634.0	−714.0	−694.0	−663.0
Corrosion rate (mmpy)	3.05×10^{-6}	7.87×10^{-6}	1.9×10^{-6}	2.79×10^{-6}

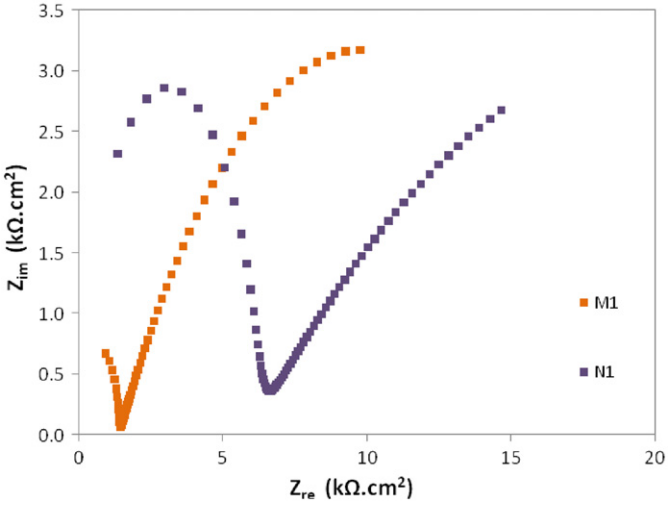

Fig. 5. Nyquist plot of micro and nanoparticle Al_2O_3-13% TiO_2 without the bonding layer.

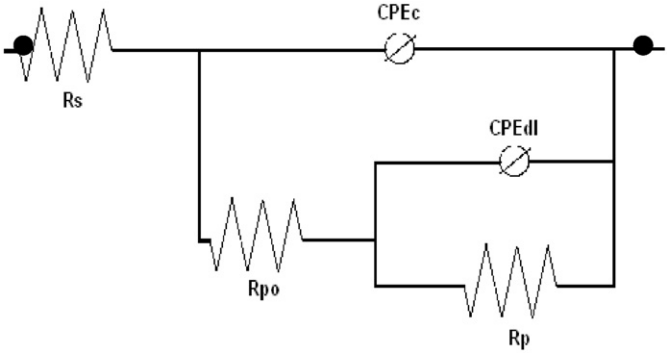

Fig. 6. Equivalent circuit for micro and nanoparticle Al_2O_3-13% TiO_2 coating without bonding layer.

immersion for 11 weeks. Fig. 5 shows the Nyquist impedance plots of microparticle and nanoparticle Al_2O_3-13% TiO_2 coatings without the metallic bonding layer (i.e., M1 and N1). Considering these typical EIS plots, as well as the studies by Gell et al [19] and Wang et al. [20] on the ceramic coating of alumina, the EIS equivalent circuit for coating without bond layer is proposed, as shown in Fig. 6, whereas the calculated parameters relevant to the impedance studies are shown in Table 4.

Based on the equivalent circuit, the impedance of the measured system between the reference electrode and the working electrode has three parts: electrolyte, ceramic layer, and interface between the ceramic and the mild steel substrates. The equivalent circuit consists of three resistance components in a series, namely, solution resistance (*Rs*), pore resistance (*Rpor*), which is the ceramic layer pore resistance revealed by the capacitance of the ceramic layer (CPE_c), and polarisation resistance (*Rp*), which is the resistance of charge transfer existing between the ceramic and mild steel interface in parallel with the double layer capacitance (*CPEdl*) [23]. The constant phase element (CPE) is a distribution parameter, indicating that the electrochemical responses of the parts of ceramic coatings do not correspond with the "pure" capacitance elements. The capacitances used in equivalent circuits are usually replaced with the CPE in the fitting of the EIS because of the coarse, inhomogeneous presence of pores exhibiting the "scattering effect." The impedance for the constant phase element is determined using Eq. (2) [24].

$$Z_{CPE} = 1/[Y_0(j\omega)^n] \quad (2)$$

where, Y_0 and n are frequency-independent fit parameters, ω ($=2\pi f$) is the angular frequency, and $j=\sqrt{-1}$. The factor n, defined as a power, is an adjustable parameter that lies between 0 and 1. If $n=0$, CPE is an ideal resistance; if $n=1$, CPE describes an ideal capacitor with Y_0 equal to the capacitance (C). The physical meaning of n remains unclear.

Fig. 7 show the Nyquist impedance plots of microparticle and nanoparticle Al_2O_3-13% TiO_2 coatings with metallic bonding layers (i.e., M2 and N2). The proposed EIS equivalent circuit for coating with the metallic bonding layer is shown in Fig. 8, and the calculated parameters relevant to the impedance studies are presented in Table 4.

As observed from the equivalent circuit, the impedance of the measured system between the reference electrode and the working electrode has four parts: electrolyte, ceramic layer, metallic bonding layer, and interface between bonding and mild steel. As a result, the equivalent circuit had additional components, such as the coating capacitance and pore resistance (*Rpor*), representing the metallic bonding layer. *Rp* and *CPEdl* were present at the interface between the metallic bonding layer and the mild steel.

The EIS fitting results, as listed in Table 4, show that the nanoparticle coatings (N1 and N2) provide better polarisation resistance (R_p) than the microparticle coatings (M1 and M2). The bond strength of the nanoparticle coating

Table 4
The optimum fitted parameters based on EIS model of equivalent circuit for M1 and N1 without bonding layer (Fig. 6) and equivalent circuit for M2 and N2 with bonding layer (Fig. 8).

	Rpo 1 (KΩ cm^2)	CPE$_c$ (MS cm^2)	n_c	Rpo 2 (Ω cm^2)	Cc (μF)	Rp (KΩ cm^2)	CPE $_{dl}$ (S cm^2)	n_{dl}
M1	1.7	2.9	0.58	–	–	12.0	6000	0.55
M2	4.3	2.5	0.57	100	200	8.0	4000	0.40
N1	6.0	1000.0	0.95	–	–	30.0	6000	0.27
N2	9.0	2.2	0.52	900	100	20.0	600	0.40

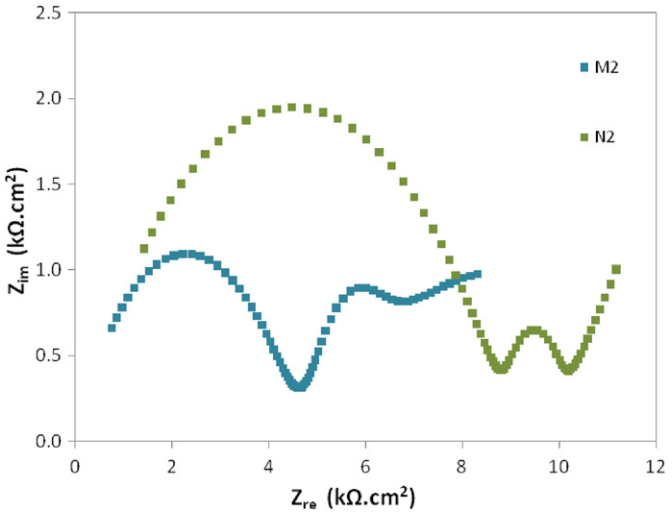

Fig. 7. Nyquist plot of the coating with the bonding layer.

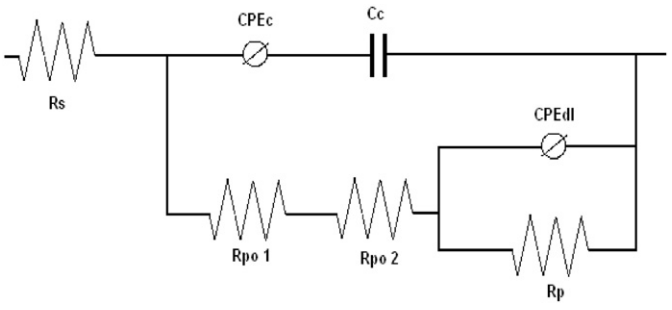

Fig. 8. Equivalent circuit for micro and nanoparticle Al_2O_3-13% TiO_2 coating with bonding layer.

was found to exhibit better bond strength compared with that of the microparticle coating [7]. High-strength bonding can prevent the coating from spallation, which decreases the R_p. The presence of the metallic bonding layer shows that the R_p decreased from 12 KΩ cm^2 to 8.0 KΩ cm^2 for the microparticle coating, whereas the nanoparticle coating decreased from 30 KΩ cm^2 to 20 KΩ cm^2 after 11 weeks of immersion. The metallic bonding layer influenced the corrosion behaviour of the coating by accelerating the corrosion process because of galvanic corrosion. The higher corrosion potential of Ni compared with that of Fe promotes the formation of galvanic corrosion on the mild steel substrate [1]. These results agree with the corrosion rate obtained from the Tafel plot extrapolation, as mentioned in Table 3.

4. Conclusion

The plasma spray method of microparticle and nanoparticle Al_2O_3-13% TiO_2 coatings on the mild steel substrate has been shown useful for controlling the rate of material degradation in specified aqueous environment. The following conclusions can be drawn from the current study. To rephrase, the conclusion can be divided into two parts:

i) Concentrating on the effect of particle size.
ii) Concentrating on the effect of metallic bonding layer.
i-a) The microparticle coating produces a small droplet splat compared with the nanoparticle coating, which increases the voids or pores of splat boundaries. The SEM image of the coating cross-section shows that the microparticle coating consists of higher pores at 8.6%. In contrast the nanoparticle coating consists of 5.0% pores.
b) The microparticle coating also provides better surface roughness than the nanoparticle coating.
c) The nanoparticle coating provides better corrosion resistance in tropical seawater because of low porosity and better bond strength.
ii-a) The presence of a metallic bonding layer reduces the pores and voids for both microparticle and nanoparticle coatings.
b) In contrast, the presence of metallic bonding layer exhibits a rough surface for both microparticle and nanoparticle coatings.
c) However, the presence of the Ni–Al metallic bonding layer diminishes the corrosion resistance resulting from galvanic corrosion.

In short, the nanoparticle ceramic coated mild steel without any metallic bonding layer is most preferable as it provides better wear corrosion resistance in tropical seawater, despite its rough surface.

References

[1] W. Tian, Y. Wang, T. Zhang, Y. Yang, Sliding wear and electrochemical corrosion behavior of plasma sprayed nanocomposite

Al_2O_3-13%TiO_2 coatings, Materials Chemistry and Physics 118 (2009) 37–45.
[2] X.Y. Wang, D.Y. Li, Application of an electrochemical scratch technique to evaluate contributions of mechanical and electrochemical attacks to corrosive wear of materials, Wear 259 (2005) 1490–1496.
[3] Y. Wang, S. Jiang, M. Wang, S. Wang, T.D. Xiao, P.R. Strutt, Abrasive wear characteristics of plasma sprayed nanostructured alumina/titania coatings, Wear 237 (2000) 176–185.
[4] J. Zhang, J. He, Y. Dong, X. Li, D. Yan, Microstructure and properties of Al_2O_3-13% TiO_2 coatings sprayed using nanostructured powders, Rare Metals 26 (2007) 391–397.
[5] R. Yilmaz, A.O. Kurt, A. Demir, Z. Tatll, Effects of TiO_2 on the mechanical properties of the Al_2O_3-TiO_2 plasma sprayed coating, Journal of the European Ceramic Society 27 (2007) 1319–1323.
[6] M. Wang, L.S. Leon, Effects of the powder manufacturing method on microstructure and wear performance of plasma sprayed alumina-titania coatings, Surface and Coatings Technology 202 (2007) 34–44.
[7] W. Tian, Y. Wang, Y. Yang, C. Li, Toughening and strengthening mechanism of plasma sprayed nanostructured Al_2O_3-13 wt% TiO_2 coatings, Surface and Coatings Technology 204 (2009) 642–649.
[8] N. Hassanuddin, M.J. Ghazali, A. Muchtar, M.C. Isa, A.R. Daud, Effects of Al_2O_3-13% TiO_2 coating particle size on commercial mild steel via plasma spray method, Key Engineering Materials 462–463 (2011) 645–650.
[9] Y. Wang, W. Tian, T. Zhang, Y. Yang, Microstructure, spallation and corrosion of plasma sprayed Al_2O_3-13% TiO_2 coatings, Corrosion Science 51 (2009) 2924–2931.
[10] J.J. Haslam, J.C. Farmer, R.W. Hopper, K.R. Wilfinger, Ceramic coatings for a corrosion-resistant nuclear waste container evaluated in simulated ground water at 90 °C, Metallurgical and Materials Transactions A 36 (2005) 1085–1095.
[11] D. Yan, J. He, X. Li, Y. Dong, Y. Liu, H. Lui, The corrosion behavior of plasma-sprayed Ni/Al–Al_2O_3 and Ni/Al-Al_2O_3 + 13 wt% TiO_2 graded ceramic coatings in 5% HCl solution, Surface and Coatings Technology 176 (2003) 30–36.
[12] S. Yilmaz, An evaluation of plasma-sprayed coatings based on Al_2O_3 and Al_2O_3-13 wt% TiO_2 with bond coat on pure titanium substrate, Ceramics International 35 (2009) 2017–2022.
[13] N.H.N. Yusoff, M.J. Ghazali, M.C. Isa, A. Muchtar, S.M. Forghani, Effect of particle size and bonding layer on plasma sprayed Al_2O_3-13% TiO_2 coatings, International Journal of Mechanical and Materials Engineering 6 (2011) 385–390.
[14] S. Yilmaz, M. Ipek, G.F. Celebi, C. Bindal, The effect of bond coat on mechanical properties of plasma-sprayed Al_2O_3 and Al_2O_3-13 wt% TiO_2 coatings on AISI 316L stainless steel, Vacuum 77 (2005) 315–321.
[15] G. Goller, The effect of bond coat on mechanical properties of plasma sprayed bioglass–titanium coatings, Ceramics International 30 (2004) 351–355.
[16] V.P. Singh, A. Sil, R. Jayaganthan, A study on sliding and erosive wear behaviour of atmospheric plasma sprayed conventional and nanostructured alumina coatings, Materials and Design 32 (2011) 584–591.
[17] Hao Du, J.H. Shin, S.W. Lee, Study on porosity of plasma-sprayed coatings by digital image analysis method, ASM International 14 (2005) 453–461.
[18] J. Zhang, J. He, Y. Dong, X. Li, D. Yan, Microstructure characteristics of Al_2O_3–13 wt% TiO_2 coating plasma spray deposited with nanocrystalline powders, Materials Processing Technology 197 (2008) 31–35.
[19] M. Gell, E.H. Jordan, Y.H. Sohn, D. Goberman, L. Shaw, T.D. Xiao, Development and implementation of plasma sprayed nanostructured ceramic coatings, Surface and Coatings Technology. 146–147 (2001) 48–54.
[20] E.H. Jordan, M. Gell, Y.H. Sohn, D. Goberman, L. Shaw, S. Jiang, M. Wang, T.D. Xiao, Y. Wang, P. Strutt, Fabrication and evaluation of plasma sprayed nanostructured alumina–titania coatings with superior properties, Materials Science and Engineering A301 (2001) 80–89.
[21] S. Yilmaz, An evaluation of plasma-sprayed coatings based on Al_2O_3 and Al_2O_3-13 wt% TiO_2 with bond coat on pure titanium substrate, Ceramics International 35 (2009) 2017–2022.
[22] J.R. Scully, Polarization resistance method for determination of instantaneous corrosion rates, Corrosion 56 (2000) 199–217.
[23] Z. Yao, Z. Jiang, S. Xin, X. Sun, X. Wu, Electrochemical impedance spectroscopy of ceramic coatings on Ti–6Al–4V by micro-plasma oxidation, Electrochimica Acta 50 (2005) 3273–3279.
[24] Y. Wang, Z. Jiang, Z. Yao, H. Tang, Microstructure and corrosion resistance of ceramic coating on carbon steel prepared by plasma electrolytic oxidation, Surface and Coatings Technology 204 (2010) 1685–1688.